Check for updates

Received: 31 January 2025 | Revised: 11 April 2025 | Accepted: 19 May 2025

DOI: 10.1111/jace.20708

Journal of the American Ceramic Society

SPECIAL ISSUE ARTICLE

From polymer to SiOC glass: structure, microstructure, mechanical, and thermal properties

Mattia Biesuz[1] | **Adane M. Abebe**[1] | **Levent Karacasulu**[1] | **Sebastiano Mariazzi**[2] | **Roberto S. Brusa**[2] | **Daria Szewczyk**[3] | **Nicola Pugno**[4,5] | **Giacomo Sero**[4] | **Maik Butterling**[6] | **Maciej Oskar Liedke**[6] | **Andreas Wagner**[6] | **Eric Hirschmann**[6] | **Michele Cassetta**[1] | **Gian D. Sorarù**[1]

[1]Department of Industrial Engineering, University of Trento, Trento, Italy

[2]Department of Physics, University of Trento, Trento, Italy

[3]Division of Low Temperature and Superconductivity, Institute of Low Temperature and Structure Research PAS, Wrocław, Poland

[4]Laboratory of Bio-Inspired, Bionic, Nano, Meta Materials & Mechanics, University of Trento, Trento, Italy

[5]School of Engineering and Materials Science, Queen Mary University of London, London, UK

[6]Helmholtz-Zentrum Dresden—Rossendorf, Institute of Radiation Physics, Dresden, Germany

Correspondence
Mattia Biesuz and Adane M. Abebe, Department of Industrial Engineering, University of Trento, Via Sommarive 9, Trento 38123, Italy.
Email: mattia.biesuz@unitn.it and adanemuche.abebe@unitn.it

Funding information
European Office of Aerospace Research and Development, Grant/Award Number: FA8655-23-1-724; National Science Centre Poland, Grant/Award Number: UMO/2024/53/B/ST3/02514

Abstract

The transformation of a methyl-siloxane into a SiOC glass in Ar and reactive CO_2 atmosphere was studied through positron annihilation spectroscopy, infrared spectroscopy, density, and calorimetric measurements, whereas the mechanical properties were monitored by nanoindentation and the thermal diffusivity measured by the laser flash method. Two types of micropores were detected at the beginning of the ceramization (700°C); one is related to the voids present in the parent polymer structure (≈0.8 nm in diameter), and the other to the polymer decomposition (≈1.2 nm in diameter at 700°C). The interconnected microporosity collapses, forming isolated pores at 800°C. These progressively sinter at higher temperatures with a final size between 0.3 and 0.7 nm at 1250°C. The porosity evolution kinetics correlates with the SiOC compositions, the densification occurring at lower temperatures in CO_2 where the matrix is close to SiO_2. However, the amorphous network obtained in Ar, leading to a heavy anionic substitution $C^{4-} \rightarrow 2O^{2-}$, is denser than that obtained in CO_2 at 1250°C. In both atmospheres, the correlation length at 1250°C is about 2.7–2.9 nm, well below the typical values of amorphous SiO_2. The porosity and structure evolution cause a progressive increase in the nanomechanical properties and thermal conductivity as the pyrolysis temperature increases. The thermal conductivity of the SiOC obtained at 1250°C in CO_2 and Ar atmosphere is about 1 and 1.8 W m^{-1} K^{-1}, respectively, such figures are symmetric to the values usually reported for amorphous silica (about 1.4 W m^{-1} K^{-1}). It is argued that the low thermal conductivity of the SiOC pyrolyzed in CO_2 is related to the presence of the free carbon phase rather than to the anionic substitution of the glass network.

KEYWORDS
characterization, polymer precursor, silicon oxycarbide, synthesis, thermal properties

This is an open access article under the terms of the Creative Commons Attribution License, which permits use, distribution and reproduction in any medium, provided the original work is properly cited.
© 2025 The Author(s). *Journal of the American Ceramic Society* published by Wiley Periodicals LLC on behalf of American Ceramic Society.

1 | INTRODUCTION

Polymer-derived ceramics (PDCs) are a class of advanced materials obtained through the pyrolysis in a controlled atmosphere of an organosilicon polymer.[1] Their chemistry, structure, and microstructure can be finely tailored by either changing the polymer composition, or the pyrolysis time, temperature, and atmosphere.[1] This has allowed to obtain ceramics and glasses with outstanding mechanical and functional properties.[2,3] As an example, silicon oxycarbide glasses showing a glass transition temperature of 1350°C have been synthesized from Si–CH_3 and Si–H containing siloxane precursors,[4] while C-rich SiOC aerogels, synthesized from a commercial siloxane and divinylbenzene display outstanding lithium storage capacity at a high charging rate (346 mAh g^{-1} at 10°C).[5]

Furthermore, a key advantage of PDCs is their possible integration with polymer-shaping technologies to obtain components that the traditional powder-based ceramics processing routes cannot produce. Examples include the integration between PDC technologies and additive manufacturing,[6,7] injection molding,[8] and spinning processes.[9,10] Through the so-called replica method, PDCs can lead to foams[11] or textured porous structures using polymeric foams or organic materials as templates.[12] The controlled gelation of Si-containing oligomers/alkoxides in a solvent can be used to obtain—after the pyrolysis process—ceramic aerogels or ambigels with outstanding thermal insulation properties and high-temperature stability.[13]

The conversion from organic into ceramic material usually involves different steps, which can be summarized as follows. First, recombination reactions take place with the evolution of silanes, then the proper ceramization occurs with methane and hydrogen evolution.[14,15] This step is associated with the formation of new chemical bonds between C (or nitrogen in the case of silazane resins) and silicon;, the material, therefore acquires an inorganic nature. The ceramization leads to an amorphous compound whose structure can be considered an anionically substituted silica, where tetrahedrally coordinated C^{4-} substitutes the linearly coordinated O^{2-}.[16,17] As the carbon and oxygen content in the polymer is not necessarily stoichiometric to obtain $SiO_{2-x}C_{x/2}$, the excess of carbon forms a segregated free carbon phase.[18,19] The evolution of gasses (silanes, H_2, methane, etc.) leaves behind some pores in the structure, which mainly fall in the microporosity range (≈1.2 nm). When the temperature further rises, the strong capillarity forces (inversely proportional to the pore size) induce viscous flow, and the material densifies.[20] Eventually, a further increase in the pyrolysis temperature causes a separation of the SiOC in oxygen-rich and carbon-rich phases, whose ultimate fate is crystallization.[21,22]

So far, PDCs have been mostly studied after pyrolysis in an inert (Ar) atmosphere. Some works have shown that pyrolysis in a reactive atmosphere (CO_2, H_2, NH_3) can change the final composition, thus impacting the short-range structure and some macroscopic properties.[23,24] It is, for instance, known that a pyrolysis in H_2 causes a selective oxidation of C–C bonds reducing the free carbon phase, while CO_2 oxidases preferentially the Si–C bonds leading to a matrix closer to SiO_2.[25–27] However, most of the work focused on the materials after the ceramization reactions when the microporosity was already closed. Just a few works investigated the closed porosity in PDCs, mainly by SAXS.[28–30] While SAXS is a valuable technique to investigate the glass structure, the information it provides is still incomplete as it reports the typical distance between electron density discontinuity, which could arise not only from the porosity but also from any local fluctuation in the material composition at the nanoscale. Besides the transient microporosity formation and closure, the evolution of the correlation distance of the glass structure during pyrolysis in different atmospheres has not been investigated yet. In summary, the medium-range evolution during the ceramization and how the atmosphere impacts it still needs to be fully understood. Indeed, the medium range is of crucial relevance as it impacts several properties from the mechanical to the thermal features.

This work aims to unravel the key features of the organic-to-inorganic transformation, focusing on medium range (≈1 nm) and the correlations between the PDCs properties (mechanical and thermal), pyrolysis temperature and atmosphere.

2 | MATERIALS AND METHODS

2.1 | Synthesis of methyl-siloxane thin film

Methyl polysiloxane (Silres MK, Wacker Chemie AG) is a silicon resin powder used as the ceramic precursor. Polysiloxane was cured at room temperature using Imidazole (CAS: 288-32-4, Merck KGaA). Xylene (CAS: 1330-20-7, Honeywell) was utilized to solubilize the silicon resin and catalyst. The composition of the solution was inspired by ref.[31]

The synthesis steps of SiOC thin film from a methyl-polysiloxane precursor are presented in Figure 1. First, MK powder (59 wt%) was mixed with xylene (40 wt%) at room temperature and stirred for 60 min by a magnetic stirrer to create a homogeneous solution. Afterward, imidazole (1 wt%) was added as a cross-linking catalyst, and the solution was stirred for a further 60 min. The resulting solution was cast using a homemade tape casting machine

15512916, 2025, 12, Downloaded from https://ceramics.onlinelibrary.wiley.com/doi/10.1111/jace.20708 by Universita Di Trento, Wiley Online Library on [08/10/2025]. See the Terms and Conditions (https://onlinelibrary.wiley.com/terms-and-conditions) on Wiley Online Library for rules of use; OA articles are governed by the applicable Creative Commons License

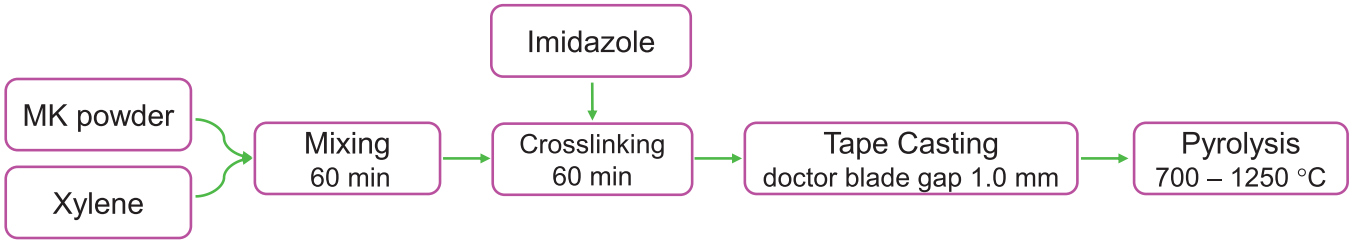

FIGURE 1 Synthesis of methyl-siloxane film from methyl-siloxane via tape casting, followed by pyrolysis in Ar/CO_2 atmosphere from 700°C to 1250°C.

with a polyethylene terephthalate carrier film with a doctor blade (gap = 1.0 mm). This film was dried at ambient temperature for 48 h before being cut into pieces. Pyrolysis was carried out at 700°C, 800°C, 900°C, and 1250°C using an alumina tube furnace (Carbolite Gero GmbH & Co. KG 75242) under argon and carbon dioxide gas flow at 100 mL min^{-1}. The samples were heated from room temperature to the pyrolysis temperature at 1°C min^{-1} and dwelled for 1 h at the maximum temperature. A cooling rate of 2°C min^{-1} was then applied under a constant gas flow.

2.2 | Characterization

Thermogravimetric analysis (TGA) was performed using a Netzsch STA 409 instrument (Netzsch-Gerätebau GmbH) under an argon and carbon dioxide flow of 100 mL min^{-1} at a heating rate of 10°C min^{-1} up to 1300°C. Approximately 90 mg of sample was placed in an alumina crucible. To eliminate oxygen residue, the furnace chamber was evacuated and refilled with gas (Ar or CO_2), repeating this cycle twice before the TGA measurement.

The bulk density, apparent density, and open porosity of the methyl-siloxane films were measured via Archimedes' principle in water using an analytical balance with a high sensitivity of $\pm 10^{-4}$ g. In addition, apparent density was also remeasured using an Ultrapyc 5000 gas pycnometer (Anton Paar GmbH). This measurement was performed at 20°C with helium gas at 18 psi target pressure. The apparent density was recorded on an average of 30 runs.

The evolution of the chemical bonds in siloxane films after pyrolysis under different atmospheres and temperatures was analyzed utilizing a Fourier transform infrared (FTIR) spectra through a thermo-optics avatar 330 instruments (Thermo Fischer Scientific) on KBr pellets. Spectra were collected in transmission mode from 400 to 4000 cm^{-1} range with 64 scans at a resolution of 4 cm^{-1}.

Carbon, silicon, nitrogen, and hydrogen contents were measured by a specialized laboratory (Mikroanalytisches Labor Pascher). The carbon concentration was assessed using a conductometric method: the sample underwent combustion, and the released CO_2 was absorbed in a NaOH solution. Si was measured by inductively coupled plasma optical emission spectrometry, ICP-OES (CIROS VISION ICP-OES, Spectro Analytical Instruments GmbH). The sample was melted in a platinum crucible using a Na_2CO_3/H_3BO_3 mixture and then dissolved in an acidic solution used for ICP. Hydrogen content was measured using infrared spectroscopy after combustion to water (H_2O). The oxygen load was estimated by subtracting the total measured components from 100.

Positron annihilation lifetime spectroscopy (PALS) at a positron implantation energy of 16 keV was carried out at the mono-energetic positron source (MePS) beamline, which is a station of the radiation source electron linac for beams with high brilliance and low emittance (ELBE) at Helmholtz-Zentrum Dresden-Rossendorf (HZDR).[32] PALS were obtained on the external surface of the PDC films. Positrons implanted in a material thermalize in a few ps and, after a diffusion path, annihilate with an electron of the medium. The PALS technique measures the lifetime of positrons in the solid, that is, the time interval between the start signal given by the pulses of MePS and the stop signal given by the annihilation gamma-ray recorded by a $CeBr_3$ scintillator detector. The total time resolution (pulsed beam and detection) is 230 ± 10 ps. More details on the detection and the data recording can be found in ref.[33]

Positrons have different fates, they can: (i) annihilate with an electron of the bulk solid; (ii) be trapped in open volume defects such as vacancy-like or vacancy clusters; and (iii) form positronium, the metastable bound state between an electron and a positron, in porosity, that is, large free volumes. Positronium is formed in two spin states: para-positronium (pPs, singlet, opposed spins) and ortho-positronium (oPs, triplet, aligned spins). In vacuum, three-fourth of Ps is formed as oPs and one-fourth as pPs. pPs has a very short lifetime of 125 ps, while oPs has a lifetime of 142 ns in the vacuum, but when it is confined into a pore, its lifetime is shortened by the so-called pick-off process. Pick-off process consists in the annihilation of the positron of the oPs with an electron of the medium with

15512916, 2025, 12, Downloaded from https://ceramics.onlinelibrary.wiley.com/doi/10.1111/jace.20708 by Universita Di Trento, Wiley Online Library on [08/10/2025]. See the Terms and Conditions (https://onlinelibrary.wiley.com/terms-and-conditions) on Wiley Online Library for rules of use; OA articles are governed by the applicable Creative Commons License

opposite spin during the bunching of oPs with the walls of the pores.

A PALS spectrum $F(t)$ is composed by a sum of exponential functions convoluted with a resolution function $R(t)$:

$$F(t) = R(t) \otimes \sum_i \frac{I_i}{\tau_i} e^{-\frac{t}{\tau_i}} + B \quad (1)$$

where τ_i and I_i are the lifetimes and the related intensities and B is the background. The intensities sum to one, and from the lifetimes the dimension of the open volumes in which positrons annihilate can be calculated. For the analysis of the spectra, a resolution function composed by two Gaussian functions with distinct intensities and centers were used. The PALS deconvolution was carried out using software PALSfit[34] (see also Figure S1).

The spectra were properly fitted (χ^2 around 1) with three lifetimes in the precursor, while a fourth lifetime was needed after pyrolysis. One of the lifetimes was fixed at 125 ps to model the presence of the pPs component for all the samples but the ones pyrolyzed at 1250°C, which showed only a modest positronium formation. The pore size was calculated from the ortho-positronium lifetimes reduced by pick-off using the equation[35]:

$$\lambda_{(R)} = \lambda_{(A)} \left[1 - \frac{R}{R + \Delta R} + \frac{1}{2\pi} \sin\left(\frac{2\pi R}{R + \Delta R}\right)\right] \quad (2)$$

where $\lambda_{(R)}$ is the inverse of the lifetime, $\lambda_{(A)} = (\lambda_S + 3\,\lambda_T)/4$ ps^{-1} with λ_S and λ_T are the annihilation rate of the singlet and triplet positronium state in vacuum, R is the pore radius, and ΔR an empirical parameter equal to 0.16 nm.

Thermal diffusivity (α) of methyl-siloxane films was measured on 10 × 10 mm square samples using a laser flash analysis (Netzsch LFA 467 HyperFlash) at temperatures up to 500°C. Before the measurement, each sample was coated with graphite to enhance light absorption and emission from the sample surfaces. The samples were then mounted on the sample holder, and measurements were taken at intervals of 50°C, beginning at 25°C, 50°C up to 500°C, with a 600 μs pulse and 250 V. Once a sample reached the target temperature, a burst of energy from a pulsed laser was absorbed by its front face, producing uniform heating. The temperature rise on the rear face was then recorded over time using an infrared detector. Thermal diffusivity was calculated with Proteus software, applying a linear penetration model based on the recorded time and temperature increase. The calculation used the relation: $\alpha = 0.1388 l^2/t_{0.5}$, where l represents the sample thickness and $t_{0.5}$ is the time at which the temperature reaches 50% of its maximum.

The nanomechanical properties of the material were determined by nanoindentation. Before the analysis, the samples were polished with SiC papers (grit 4000) and 1 μm diamond paste. Nanoindentation was performed in the bulk of the material (i.e., far from the surface). This method is used to characterize materials in all forms, including bulk samples, thin films, multiphase materials, polymers, ceramics, metals, and biomaterials. While the procedures to control the experiment are somewhat complex, it is simple to use and based on the classical Oliver and Pharr method. It is designed to provide a simple, constant indentation strain rate test technique for measuring the elastic modulus and hardness of a material as a function of depth. The primary inputs are the Poisson's ratio of the sample being tested and the target depth at which the loading will stop. This indentation method is used to measure the mechanical properties of the sample continuously as the indenter is forced into the surface. A constant dynamic displacement excitation is used to measure the stiffness of the contact as the load is increased. The resulting set of parameters (LOAD, DEPTH, and STIFFNESS) are used (with the Oliver and Pharr method) to calculate the hardness and elastic modulus of the sample continuously as the load is increased. By default, the indentation strain rate is 1.0 s^{-1}, and there is no thermal drift segment as the total test time is minimal; the Poisson's ratio is fixed at 0.11 and 0.13 for Ar and CO_2 pyrolyzed samples.

The specific heat was measured using a standard thermal relaxation method implemented in the heat capacity option with a Physical Property Measurement System—Quantum Design PPMS. Before each sample's specific heat experiment, an additional measurement took place to exactly subtract the background contribution. The samples used for the experiment were cut from bulk specimens with final masses ranging from 0.5 up to 3 mg. Detailed information on the measuring method, analysis, and sample connections can be found in refs.[36, 37]

The correlation length was calculated from the Boson peak (BP) position and the elastic properties using:

$$\xi = \frac{\upsilon_T}{\omega_{BP}} \quad (3)$$

where υ_T is the transverse sounds velocity and ω_{BP} is the BP position frequency. Low-temperature calorimetric measurements are not influenced by rules that select specific vibrational modes. Instead, they respond to the total number of vibrational states ($g(\omega)/\omega^2$) that affect heat capacity. This makes them a valuable reference for studying vibrational excitations in the THz range using inelastic scattering. Following, we calculated the C_p/T^3 maximum as a function of T, namely T^{max},[38] as the BP in the $g(\omega)/\omega^2$ with ω_{BP} in cm^{-1} according to the Einstein model for the

15512916, 2025, 12, Downloaded from https://ceramics.onlinelibrary.wiley.com/doi/10.1111/jace.20708 by Universita Di Trento, Wiley Online Library on [08/10/2025]. See the Terms and Conditions (https://onlinelibrary.wiley.com/terms-and-conditions) on Wiley Online Library for rules of use; OA articles are governed by the applicable Creative Commons License

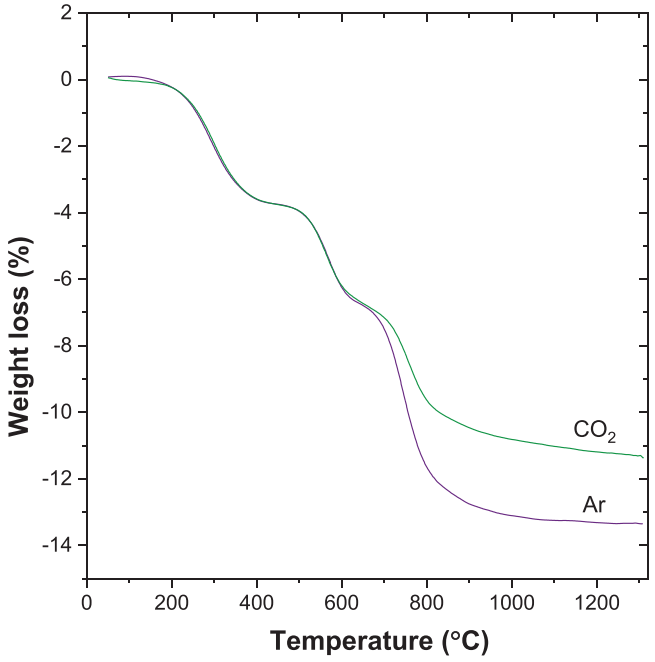

FIGURE 2 Thermogravimetric analysis (TGA) of methyl-siloxanes films pyrolyzed in Ar and CO_2.

heat capacity as[38]:

$$T^{\max} = \frac{1}{39\,763}\left(\frac{\omega_{BP}}{k_B}\right) \quad (4)$$

where k_B is the Boltzmann constant. and the transverse sound velocity from the elastic properties and density of the material:

$$\upsilon_T = \left(\frac{G}{\rho}\right)^{0.5} \quad (5)$$

where G is the shear modulus and ρ is the density. Assuming an isotropic medium $G = E/[2(1+\nu)]$, where E is the elastic modulus and ν is the Poisson ratio. E was taken from the nanoindentation data. The Poisson ratio for the SiOC obtained in Ar was assumed to be 0.11,[39] whereas it was assumed to be slightly larger in CO_2 (0.13) as the matrix is shown to be closer to SiO_2. However, given the uncertainties of ν in the SiOC systems,[40] we calculated the correlation length resulting from two limiting scenarios $\nu = 0.1$ and 0.2. As it will be shown the impact on the final result is relatively modest.

3 | RESULTS

The TGA plots in Figure 2 reveal three major steps in the pyrolysis process. The first drop at ≈300°C is associated with the evolution of residual solvent and oligomers. The 500°C–600°C region is typically dominated by the recombination reactions with the release of silanes, whereas the mineralization occurs mainly between 700°C and 900°C and is associated with the evolution of hydrocarbons and H_2. Pyrolysis both in CO_2 and Ar follow a similar trend though the weight loss seems generally more limited in carbon dioxide likely because of the partial oxidation of the sample. In general, the step that appears more affected by the atmosphere is the third one, that is, ceramization.

The composition of the SiOC films and the precursor are reported in Figure 3, and the data are summarized in Table 1. The composition change is already substantial at 700°C in Ar, with a robust decrease in the H content compared with the pre-ceramic precursor, whereas a much larger amount of H is retained in CO_2. At higher temperatures, the H content quickly drops in CO_2, and is even lower than that in Ar at 900°C. Finally, at 1250°C, the H remaining in the system is nearly negligible in both the atmospheres. The O and C content also evolve with temperature. First, we can spot that up to 800°C the C content decreases consistently with the evolution of silanes, such as $Si(CH_3)_4$, methane, and other low-molecular-weight hydrocarbons. At higher temperatures, the C content is stable, suggesting that the mineralization occurs mainly through the release of H_2. In general, the sample pyrolyzed in CO_2 contains a higher amount of O. The final SiOC stoichiometry based on the chemical analysis is $SiC_{0.1}O_{1.80} + 0.67C_{free}$ in CO_2 and $SiC_{0.23}O_{1.54} + 0.55C_{free}$ in Ar.

The FTIR spectra depict the inorganic network formation as the pyrolysis temperature increases (Figure 4). Specifically, we observe a decrease of the C–H-related features at 1277 and 2975 cm^{-1}, which disappear at 900°C. Still, some weak C–H bending and stretching signals can be observed at 700°C and 800°C. These appear stronger when the pyrolysis is carried out in CO_2. At temperatures above 900°C, only the vibrational features of Si–O and Si–C can be detected. Comparing the spectra of the samples pyrolyzed at 1250°C, we can observe that the centroid of the Si–O–Si asymmetric stretching peak does not shift, but pyrolysis in CO_2 leads to a stronger tail in the high wavenumber region.

The conversion of the organic into an inorganic SiOC caused a substantial density evolution, which was followed both by He-pycnometry and Archimedes' density measurements (Figure 5). Both apparent and bulk density monotonically increase with pyrolysis temperature. At 700°C, the samples pyrolyzed in Ar are significantly denser than the ones obtained in CO_2, and some open porosity was detected by Archimedes' method. At 800°C, such open porosity completely disappears. At 800°C and 900°C, the density in Ar and CO_2 are rather similar. Finally, the density of the sample pyrolyzed in Ar is substantially larger than that in CO_2 at 1250°C.

15512916, 2025, 12, Downloaded from https://ceramics.onlinelibrary.wiley.com/doi/10.1111/jace.20708 by Universita Di Trento, Wiley Online Library on [08/10/2025]. See the Terms and Conditions (https://onlinelibrary.wiley.com/terms-and-conditions) on Wiley Online Library for rules of use; OA articles are governed by the applicable Creative Commons License

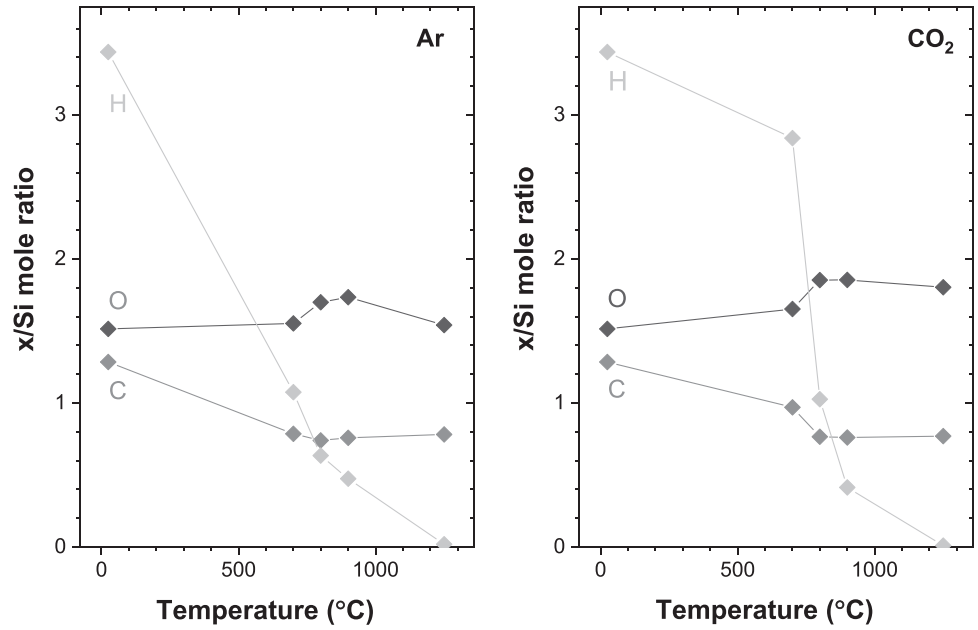

FIGURE 3 Chemical composition of the methyl-siloxane films pyrolyzed in different atmospheres.

TABLE 1 Chemical analysis of methyl-siloxane film pyrolyzed from 700°C to 1250°C in Ar and CO_2.

	Molar ratio				
T (°C)	O/Si	C/Si	H/Si	Empirical formula	Oxycarbide stoichiometry
Carbon dioxide					
25	1.51	1.28	3.44	$SiC_{1.28}O_{1.51}H_{3.44}$	
700	1.65	0.97	2.84	$SiC_{0.97}O_{1.65}H_{2.84}$	
800	1.85	0.77	1.03	$SiC_{0.77}O_{1.85}H_{1.03}$	
900	1.86	0.76	0.41	$SiC_{0.76}O_{1.86}H_{0.41}$	
1250	1.80	0.77	0.01	$SiC_{0.77}O_{1.80}H_{0.01}$	$SiC_{0.1}O_{1.80} + 0.67C_{free}$
Argon					
25	1.51	1.28	3.44	$SiC_{1.28}O_{1.51}H_{3.44}$	
700	1.55	0.79	1.08	$SiC_{0.79}O_{1.55}H_{1.08}$	
800	1.70	0.74	0.64	$SiC_{0.74}O_{1.70}H_{0.64}$	
900	1.74	0.76	0.47	$SiC_{0.76}O_{1.74}H_{0.47}$	
1250	1.54	0.78	0.02	$SiC_{0.78}O_{1.54}H_{0.02}$	$SiC_{0.23}O_{1.54} + 0.55C_{free}$

PALS spectra reveal the microstructural evolution of the PDC during the pyrolysis process (Figure 6). The precursor can be modeled using three lifetimes. The first (τ_1) was fixed to the lifetime of para-positronium (≈125 ps). The other two lifetimes arise from the positron annihilation with electrons of the bulk ($\tau_2 \approx 0.45$ ns) and from the pick-off annihilation of oPs in the larger free volumes between the polymer ladder chains ($\tau_3 \approx 3.4$ ns). The size of these larger voids is in the order of 0.8 nm using Equation (2). When pyrolysis is carried out at 700°C, some new porosity forms, resulting in a more opened network compared to the pre-ceramic precursor. These new pores that arise from the decomposition of the polymer are associated with a new lifetime $\tau_4 \approx 8$ ns (about 1.2 nm). The relative amount of this new class of pores is larger in CO_2 than in Ar. However, it quickly relaxes and the intensity associated with a τ_4 drops in CO_2 between 700°C and 900°C, whereas its intensity decreases gently in Ar. Throughout the pyrolysis process, the response of the bulk of the material in terms of lifetime does not change, τ_2 always being ≈0.45 ns. The intensity ($I_4 + I_3$) of oPs in samples treated at 1250°C reduces to about 8%–12%, and the pPs component vanishes below the sensibility of the fitting procedure. Interestingly, we can observe the sintering of the micropores, which is associated not only with a decrease in τ_3 and τ_4 intensity but also with a reduction in their

15512916, 2025, 12, Downloaded from https://ceramics.onlinelibrary.wiley.com/doi/10.1111/jace.20708 by Universita Di Trento, Wiley Online Library on [08/10/2025]. See the Terms and Conditions (https://onlinelibrary.wiley.com/terms-and-conditions) on Wiley Online Library for rules of use; OA articles are governed by the applicable Creative Commons License

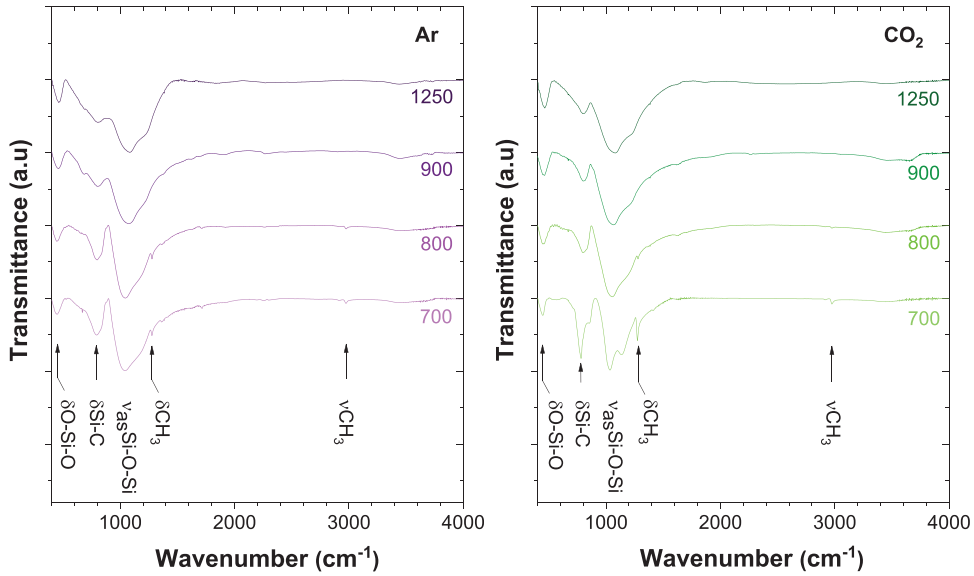

FIGURE 4 Fourier transform infrared (FTIR) spectra of the methyl-siloxane pyrolyzed in different atmospheres.

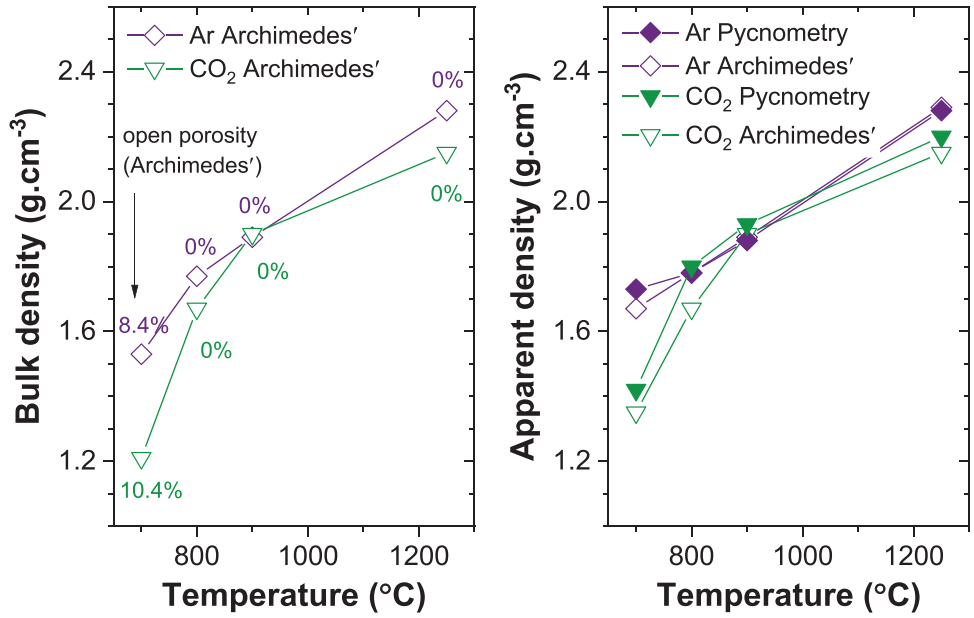

FIGURE 5 Density and porosity measurements as a function of the pyrolysis temperature in Ar and CO_2.

lifetimes, signaling a reduction of the pore size (Figure 7). At 1250°C, the positronium-related annihilation events possess a lower intensity (i.e., I_3 and I_4) in Ar than in CO_2, revealing that the SiOC obtained in Ar contains a smaller amount of free volumes. While the dynamic of the intensities evolution with temperature is substantially different in the two atmospheres, the pore size is rather similar in Ar and CO_2, with a final size of the free volumes reduced to 0.3–0.7 nm in both environments.

The nano-hardness (H) and indentation modulus (E) of the films are reported in Figure 8. Both H and E increase with the pyrolysis temperature. The mechanical properties at 700°C are substantially higher when the pyrolysis is carried out in Ar coherently with the lower porosity detected by PALS and Archimedes' method. The rapid reduction of the pore volume and related density increase in CO_2 between 700°C and 900°C causes a remarkable increase in E and H, which, at 900°C, are rather similar in the two pyrolysis atmospheres. Eventually, at 1250°C H and E in Ar are larger than in CO_2, reflecting the denser and highly polymerized structure of the SiOC. The modulus obtained for the sample pyrolyzed in CO_2 (≈80 GPa) is not

15512916, 2025, 12, Downloaded from https://ceramics.onlinelibrary.wiley.com/doi/10.1111/jace.20708 by Universita Di Trento, Wiley Online Library on [08/10/2025]. See the Terms and Conditions (https://onlinelibrary.wiley.com/terms-and-conditions) on Wiley Online Library for rules of use; OA articles are governed by the applicable Creative Commons License

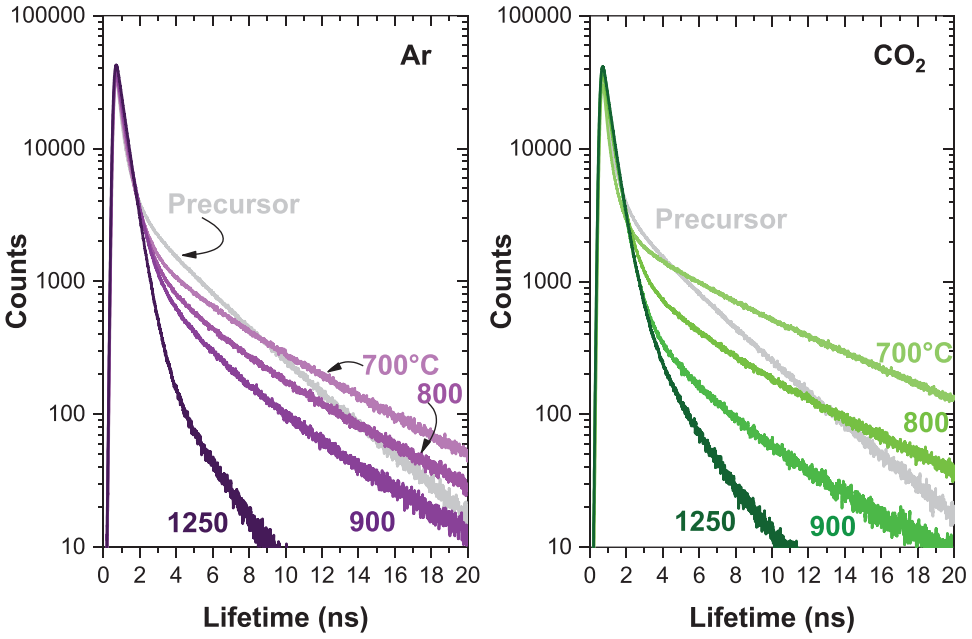

FIGURE 6 Positron annihilation lifetime spectroscopy (PALS) spectra of methyl-siloxane films pyrolyzed in Ar and CO_2 atmosphere at different temperatures.

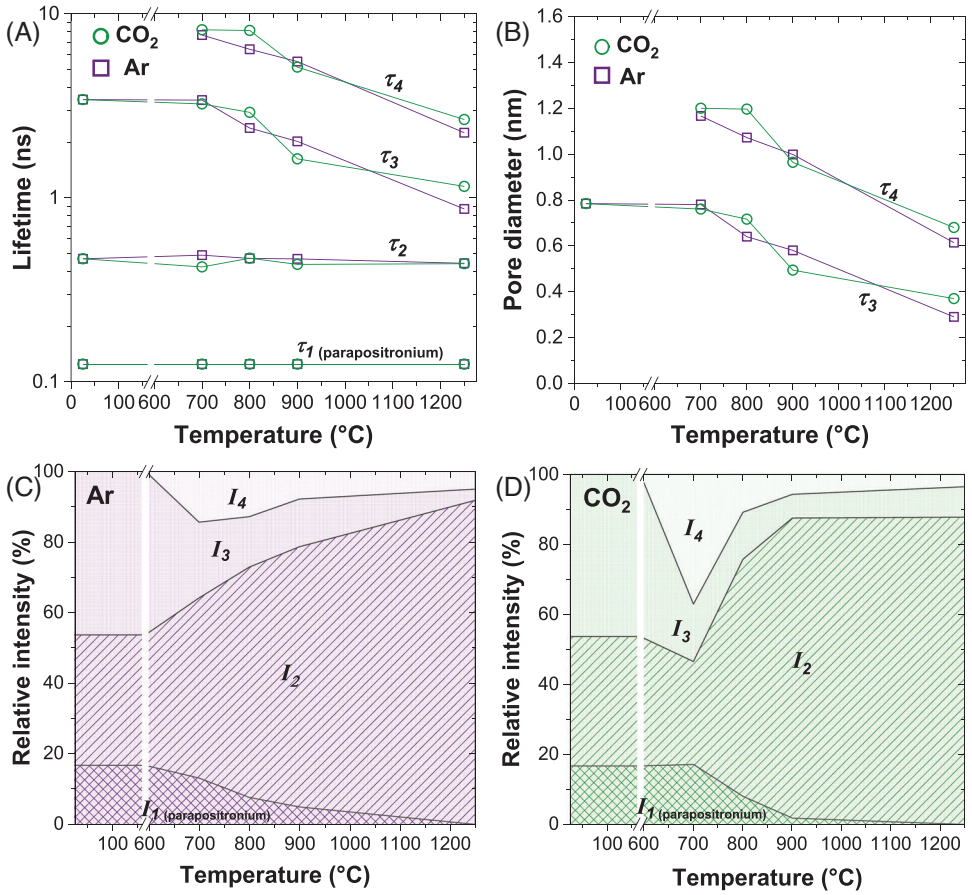

FIGURE 7 (A) Lifetimes, (B) pore radius, and (C and D) associated intensities obtained by the deconvolution of the spectra in Figure 6.

15512916, 2025, 12, Downloaded from https://ceramics.onlinelibrary.wiley.com/doi/10.1111/jace.20708 by Universita Di Trento, Wiley Online Library on [08/10/2025]. See the Terms and Conditions (https://onlinelibrary.wiley.com/terms-and-conditions) on Wiley Online Library for rules of use; OA articles are governed by the applicable Creative Commons License

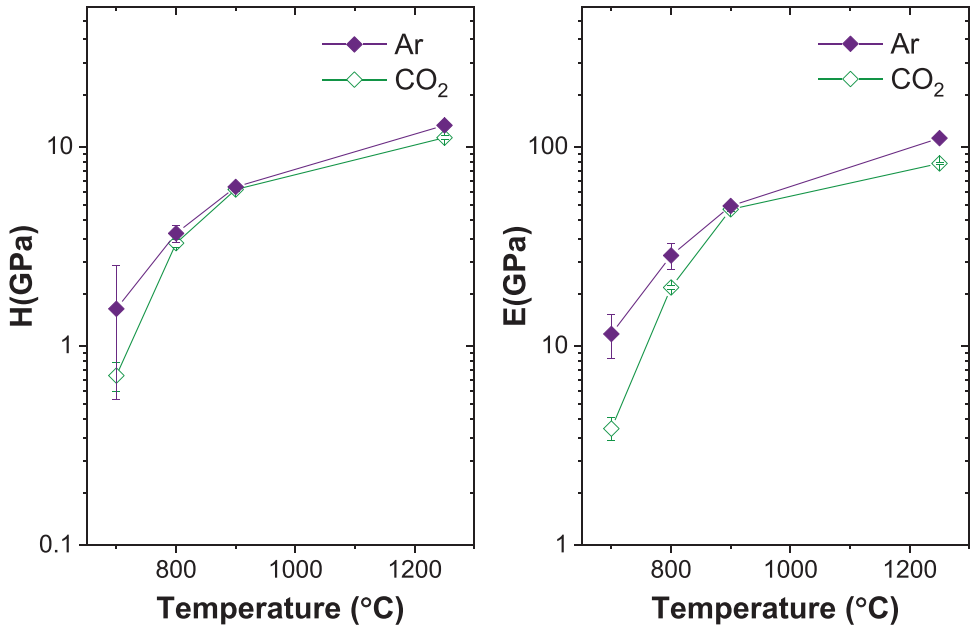

FIGURE 8 Nano-hardness and elastic modulus for methyl-siloxane films pyrolyzed at different temperatures in Ar and CO_2.

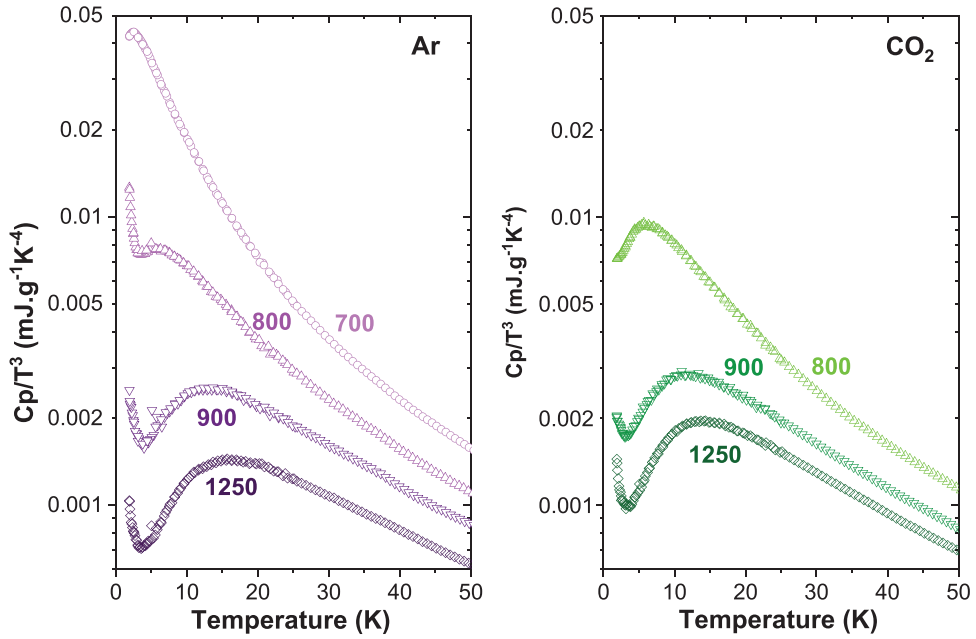

FIGURE 9 Debye-reduced specific heat of methyl-siloxane film pyrolyzed in Ar and CO_2 at different temperatures.

far from what would be expected for a network similar to silica[41–43] and agrees with previous results obtained in the SiOC system pyrolyzed in CO_2.[24]

Figure 9 reports the specific heat of the precursor together with the data of pyrolyzed samples at different temperatures and atmospheres. Due to a very small thermal response of the CO_2 pyrolyzed sample at 700°C during the experiment, this case was excluded from the analysis. The specific heat data in Figure 9 are represented in Debye-reduced coordinates—namely C_p/T^3 versus T. One can observe that in both atmospheres, increasing the temperature of the pyrolysis lowers the value of the heat capacity implying a decreasing order within the structure. Additionally, with increasing the pyrolysis temperature, the position of the BP shifts from 2.5, 5, 12 up to 15 K in the case of the Ar, and from 6, 10 up to almost 14 K for the CO_2 case.

15512916, 2025, 12, Downloaded from https://ceramics.onlinelibrary.wiley.com/doi/10.1111/jace.20708 by Universita Di Trento, Wiley Online Library on [08/10/2025]. See the Terms and Conditions (https://onlinelibrary.wiley.com/terms-and-conditions) on Wiley Online Library for rules of use; OA articles are governed by the applicable Creative Commons License

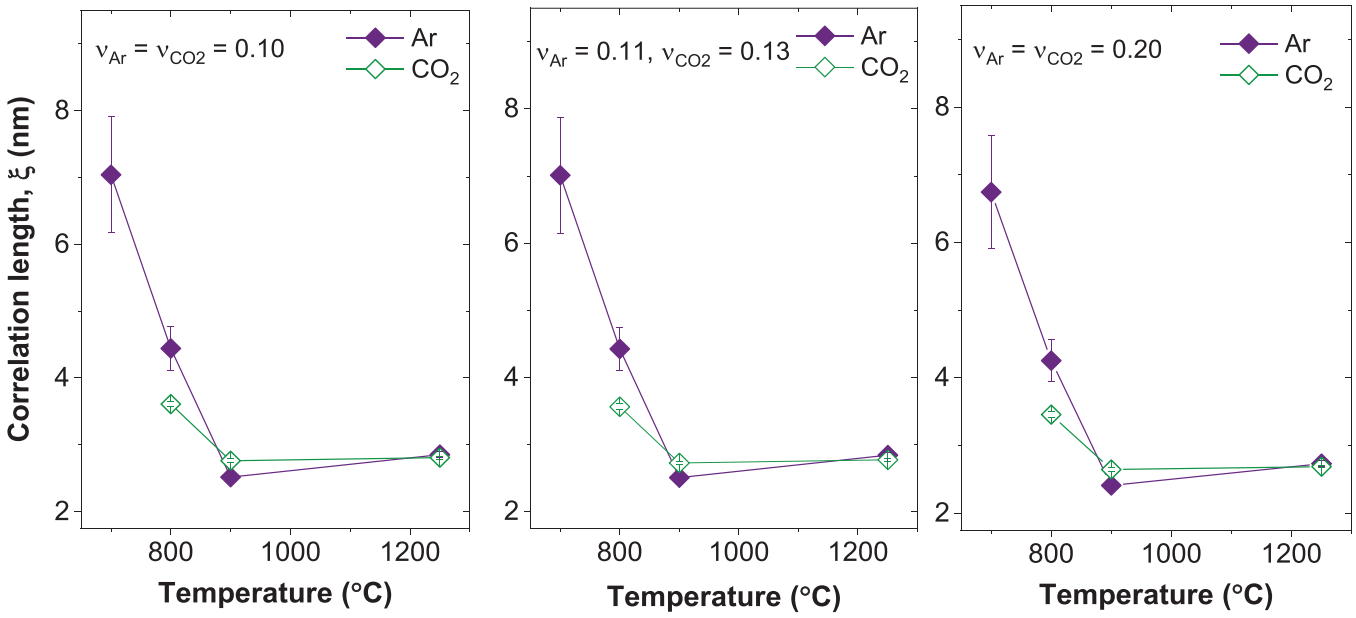

FIGURE 10 Correlation length as a function of the pyrolysis temperature and atmosphere for different Poisson ratios.

The combination of the calorimetric BP data (Figure 9) and the elastic properties (Figure 8) allows the calculation of the correlation length, ξ (Figure 10), representing the distance over which the short-range order of the amorphous structure is lost. Given the uncertainty in the Poisson ratio, Figure 10 reports the correlation length assuming different values of ν. We can observe that the differences are relatively modest, even varying ν in a wide range from 0.1 to 0.2. At 700°C the correlation length (around 7 nm) is relatively long. During the ceramization process, there is a structural evolution increasing the disorder in the system, which is completed at 900°C. Between 900°C and 1250°C, the evolution is modest, and the final correlation length only marginally increases. In both atmospheres, the final correlation length is around 2.7–2.9 nm, which is significantly lower than that of pure SiO_2 glass (3.9–4.4 nm).[44,45]

The thermal diffusivity measured by the laser flash method at different temperatures is reported in Figure 11 (top panels). Its value increases significantly with the pyrolysis temperature as a result of the structural evolution of the PDC network. Note that it was not possible to assess the thermal diffusivity of the film pyrolyzed at 700°C in CO_2 due to the sample's insufficient mechanical integrity.

The thermal conductivity was derived from the diffusivity data using the specific heat calculated with the Neumann–Kopp rule from the film's elemental composition, the results are shown in Figure S2. To strengthen the application of the Neumann–Kopp model to SiOC systems, we compared the computed C_p with literature values for SiC, SiO_2, and SiOC[46] (Figure S3). The model provides an acceptable approximation of the experimental results from the literature with an average deviation of 0.01% for SiC, 0.06% for SiO_2, and 0.02% for SiOC.

The thermal conductivity (Figure 11, bottom panels) increases with temperature, reaching a saturation value for all the systems, similar to other amorphous materials. The pyrolysis temperature causes a substantial increase in the conductivity of the materials as a result of the porosity evolution, and the properties are substantially different in the two atmospheres. Specifically, the thermal conductivity is higher in the samples pyrolyzed in an inert gas. The thermal conductivity of samples pyrolyzed in CO_2 is substantially lower, and the values are well below what would be expected for SiO_2 glass. For instance, the thermal conductivity of amorphous silica at room temperature is expected to be around 1.4 W m^{-1} K^{-1},[47] whereas the sample pyrolyzed in CO_2 at 1250°C in this work showed a conductivity of only about 0.8 W m^{-1} K^{-1} and only at 500°C it approaches 1.2 W m^{-1} K^{-1}.

4 | DISCUSSION

The conversion of methyl-siloxane films into a SiOC glass is substantially affected by the pyrolysis atmosphere; pyrolysis in CO_2 leads to a glass matrix, embedding a nano-dispersed free carbon phase, chemically close to amorphous SiO_2 at 1250°C.[25–27,49] On the other hand, the pyrolysis in an inert atmosphere (Ar) causes the formation of a SiOC glass network containing Si–O and Si–C bonds. This is confirmed by the chemical analysis (Table 1) and supported by the shape of the main vibrational feature of tetrahedrally coordinated Si in the FTIR spectra (Figure 4),

15512916, 2025, 12, Downloaded from https://ceramics.onlinelibrary.wiley.com/doi/10.1111/jace.20708 by Universita Di Trento, Wiley Online Library on [08/10/2025]. See the Terms and Conditions (https://onlinelibrary.wiley.com/terms-and-conditions) on Wiley Online Library for rules of use; OA articles are governed by the applicable Creative Commons License

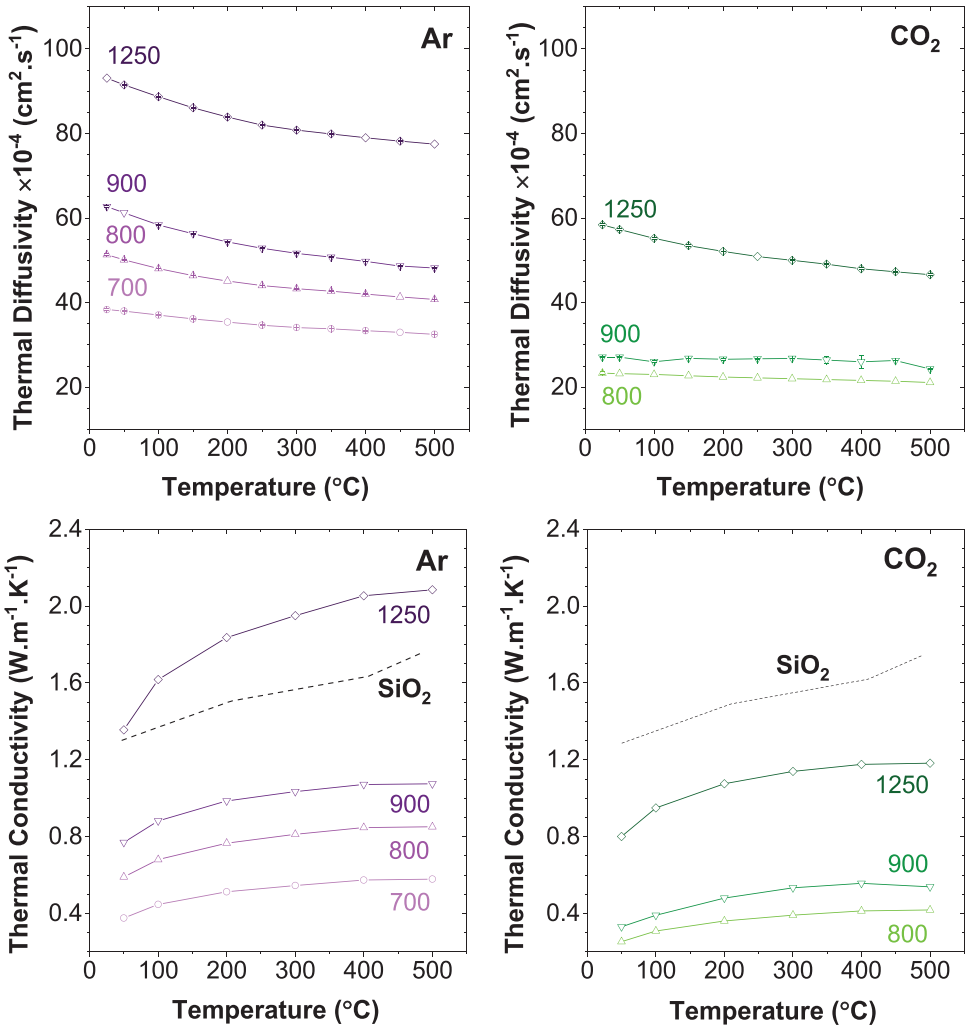

FIGURE 11 Thermal diffusivity and conductivity for methyl-siloxane films pyrolyzed at different temperatures in Ar and CO_2. The data for amorphous SiO_2 are taken from ref.[48]

that is, the stretching (1000–1200 cm^{-1}) of the tetrahedral Si coordinated by carbon are red-shifted when compared to silica. In general, these results match what would be expected from the literature.[25–27,49]

On the other hand, some "unexpected" results can be evinced in this work: (i) at 700°C, the pyrolysis in CO_2 causes the formation of a transient micro-porosity (1.2 nm) whose amount and size abundantly surpasses those formed in Ar atmosphere; (ii) the pyrolysis in CO_2 seems delayed, with still a large amount of H present at 700°C (Table 1 and Figure 3). It has been reported that CO_2 is reactive toward the Si–CH_2–Si or Si–CH_2–CH_2–Si bonds, which form at the early stage of ceramization.[27] The reactivity of CO_2 at a relatively low temperature (i.e., 700°C) is confirmed by the substantial increase in the oxygen content compared with both the pre-ceramic precursor and the sample pyrolyzed in Ar at 700°C (Table 1 and Figure 3). In previous work,[27] where a highly polymerized $SiO_{1.5}CH_3$ system has been used, the differences in the FTIR spectra at 700°C are very mild, but still, a slightly larger amount of –CH_3 can be spotted in CO_2. One could note that the system in this work is less polymerized and contains a relatively large amount of unreacted alkoxides (Si–OR). In fact, the C/Si ratio in the precursor is 1.28, larger than the theoretical one of a fully polymerized material. The residual alkoxide groups or their decomposition products might play a role and react with the CO_2. The mechanistic understanding of the reactions involved in CO_2 is, however, still not fully clarified and deserves specific work to be unraveled.

The microstructure evolution of the films in the two different atmospheres can be evinced by combining the results from PALS and density measurement. At 700°C, a new lifetime, τ_4, appears as a result of the silane release during the redistribution reactions and is associated with pores of about 1.2 nm in diameter. On the other hand, the "large free volumes" present in the polymer structure, pointed out by τ_3, I_3, remain without a substantial change

15512916, 2025, 12, Downloaded from https://ceramics.onlinelibrary.wiley.com/doi/10.1111/jace.20708 by Universita Di Trento, Wiley Online Library on [08/10/2025]. See the Terms and Conditions (https://onlinelibrary.wiley.com/terms-and-conditions) on Wiley Online Library for rules of use; OA articles are governed by the applicable Creative Commons License

in their size (≈0.8 nm), and concentration, that is, the lifetime and the related intensity does not change up to 700°C. The free volume starts to decrease both in size and concentration from 800°C (lifetime and intensity reduction Figure 7). The response of the bulk (τ_2) is stable in terms of lifetime and is representative of small ring structures falling below the positronium formation onset (i.e., the positron annihilates directly with the electron without positronium formation). As the number of free volumes and pores decrease with the pyrolysis process (I_3 and I_4 decrease) positron annihilate more in a bulk state (increase of I_2)

While a large amount of porosity is formed in CO_2 at 700°C, it is less stable than in Ar, and the material undergoes a substantial densification between 700°C and 900°C (see Figure 7, relative intensity). In the samples treated in the Ar atmosphere, the concentration of free volumes and pores decreases more slowly, and only at 1250°C is comparable with that in samples treated in CO_2. On the contrary, the size of free volumes and pores decreases both in the samples treated in Ar and in CO_2.

The differences in the pore evolution can be explained by the different resistance to the viscous flow of the two materials. In fact, the SiOC obtained in Ar is expected to possess a higher viscosity than the CO_2 counterpart due to a more "polymerized" glassy matrix related to the $C^{4+} \rightarrow 2O^{2-}$ anionic substitution. Actually, SiOC is known to possess a viscosity about 2 orders of magnitude larger than SiO_2 glass and its glass transition temperature (T_g) of about 1350°C, which is roughly 150°C above the T_g of SiO_2.[50]

The densification is indeed driven by the surface tension of the micro-pores able to activate viscous flow at relatively low temperatures. At 800°C, no open (interconnected) porosity can be detected in both atmospheres, while clearly closed pores remain in the systems as depicted by the PALS spectra. Therefore, between 700°C and 800°C, the interconnected porosity collapses in isolated closed pores due to the Rayleigh instability. The existence of such closed pores is confirmed by the presence of long lifetimes in the PALS spectra and by the fact that the samples still experience a density evolution above 800°C. Remarkably, we were able to monitor for the first time the sintering of the transient closed microporosity in PDCs by PALS, the sintering event being associated with a reduction of τ_3 and τ_4 intensity and in a shortening of these lifetimes (smaller micro-pores). At 1250°C, the pores are in the order of about 1 nm. The substantial densification agrees with the density evolution measured by pycnometry and Archimedes' method and with the hardness (H) and elastic modulus (E) evolution revealed by the nanoindentation measurements.

At 1250°C, PALS results suggest that the SiOC obtained in Ar is characterized by a lower amount of free volume compared to the one obtained in CO_2 (the intensities related to oPs in Ar is about 3%–4% lower than in CO_2). The conclusion is corroborated by the density measurements highlighting that the density in Ar is higher. Hence, we can infer that the anionic substitution of $C^{4-} \rightarrow 2O^{2-}$ in the Ar-pyrolyzed SiOC (bearing in mind that the glass obtained in CO_2 is closer to SiO_2), causes a substantial densification of the amorphous network. The conclusion seems reasonable considering the larger coordination of carbidic C (fourfold) compared with that of oxygen ions (twofold).

The correlation length (ξ) during the pyrolysis process drops between 700°C and 900°C, while a modest increase can be observed between 900°C and 1250°C. The drop in the first part of the pyrolysis is consistent with previous results by SAXS on a more polymerized $SiO_{1.5}CH_3$[20] and originates from the fact that the methyl-siloxane precursor often organizes itself in relatively regular structures (for instance, ladder-like). The parent order of the preceramic polymer is partially retained at low temperatures and is totally lost at 900°C when the material is fully ceramized, thus resulting in a drop in the correlation length. The final correlation length at 1250°C is similar for both atmospheres and is between 2.5 and 3 nm. Such a distance is smaller than what was measured in SiO_2 (3.9–4.4 nm).[44,45] One might argue that the anionic substitution of $C^{4+} \rightarrow 2O^{2-}$ causes the development of a more disordered network thus decreasing ξ. Similar cases exist in the literature for cationic substitution, for instance, the addition of Al_2O_3 to SiO_2 decreases ξ from ≈3.9 nm (pure SiO_2) to ≈3.35 nm (7 mol% Al_2O_3). However, herein, similar correlation lengths have been obtained in Ar and CO_2; in other words, SiOC glasses with far different content of carbidic carbon show similar ξ. Based on this observation, the other possible explanation is that the correlation length of the polymer-derived SiOC is not controlled by the C^{4-} in solid solution but by the presence of the nano-dispersed free carbon phase whose scale is actually in the order of 2–3 nm.[51]

The density/porosity evolution correlates with the properties of the SiOC glass. Hardness and indentation modulus are larger for the samples pyrolyzed in Ar at 700°C due to the large amount of porosity developed in CO_2. However, due to the fast densification of the CO_2-pyrolyzed materials the mechanical properties become nearly identical at 900°C for both atmospheres. Eventually, the densification of the SiOC network produced in Ar between 900°C and 1250°C causes a further improvement of the mechanical properties. The final hardness/elastic modulus after pyrolysis in Ar is, therefore, higher than those obtained in CO_2. Such a result is coherent with the formation of a denser and more polymerized SiOC in Ar atmosphere. We can also spot that the H and

15512916, 2025, 12, Downloaded from https://ceramics.onlinelibrary.wiley.com/doi/10.1111/jace.20708 by Universita Di Trento, Wiley Online Library on [08/10/2025]. See the Terms and Conditions (https://onlinelibrary.wiley.com/terms-and-conditions) on Wiley Online Library for rules of use; OA articles are governed by the applicable Creative Commons License

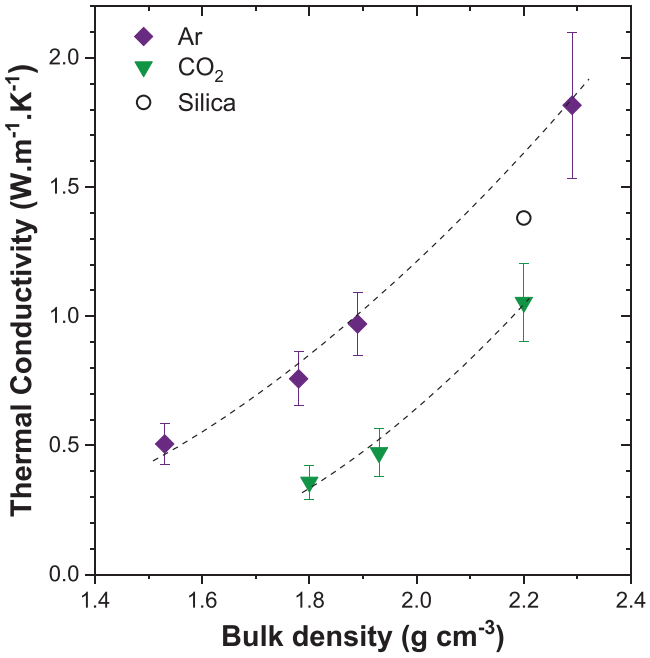

FIGURE 12 Average thermal conductivity (RT-500°C) of SiOC films pyrolyzed in Ar and CO_2 as a function of the bulk density. The conductivity of SiO_2 is reported for comparison (≈RT). The dashed lines are guides for the eye.

E increase not only because of the porosity evolution with temperature but also as a result of the polymerization of the structure through the release of hydrogen/methane and the formation of Si–O–Si and Si–C–Si bonds.

The thermal conductivity of the films evolves as a function of temperature as a result of the SiOC densification at high temperatures (Figure 12). The relatively low thermal conductivity of different PDCs systems, sometimes even lower than that of fused SiO_2, has been debated in the literature.[48,52–56] It has been often argued that the anionic substitution in PDCs could decrease the thermal conductivity by increasing the degree of disorder of the system or by changing the amount of free volume. The comparison between the data obtained in Ar and CO_2 (Figure 12) points out that this might not always be a valid argument. In fact, at a given density value SiOC obtained in Ar is definitively more conductive than in CO_2. In other words, the thermal conductivity is lower when the glass matrix is closer to silica (lower amount of anionic $C^{4-} \rightarrow 2O^2$ substitution in CO_2, Table 1). Still, our results confirm that PDCs even pyrolyzed at 1250°C could possess a thermal conductivity lower than SiO_2, but only when the pyrolysis is carried out in CO_2. As this cannot be justified by the modest $C^{4-} \rightarrow 2O^2$ substitution for the argument discussed above, we can infer that the free carbon phase, generally dispersed in tiny nanodomains, might contribute to increased phonon scattering and reduce the heat transport throughout the solid.

5 | CONCLUSIONS

The pyrolysis of methyl-siloxane in Ar and CO_2 causes the formation of a transient microporosity, which was clearly detected at 700°C. The microporosity can be divided into two classes: the first originates from voids present in the parent polymer (≈0.8 nm in diameter), and the second is formed through the ceramization process (≈1.2 nm in diameter). The porosity quickly relaxes in CO_2 due to the lower viscosity of the glass matrix (close to SiO_2), whereas it is more stable in Ar (the viscosity is expected to be larger due to the presence of carbidic C). Starting from 800°C, the porosity is fully closed (no interconnected cylindrical pores), although it is still present as closed pores depicted by PALS. Increasing the pyrolysis temperature causes a reduction of both the porosity volume and size. At 1250°C, the SiOC obtained in Ar is denser than those in CO_2. The correlation length of the glass decreases until 900°C where the ceramization is substantially completed, and only modest changes occur between 900°C and 1250°C. The correlation length in both CO_2 and Ar is about 2.7–2.9 nm, significantly lower than that of silica glass.

The structural changes correlate with the evolution of the indentation modulus, hardness, and thermal conductivity, which monotonically increase between 700°C and 1250°C and are generally higher in Ar atmosphere. At 1250°C, the thermal conductivity of fused SiO_2 lays between the ones of $SiC_{0.1}O_{1.80} + 0.67C_{free}$ (CO_2) and $SiC_{0.23}O_{1.54} + 0.55C_{free}$ (Ar). It is inferred that the low thermal conductivity in CO_2 is related to the presence of the free carbon phase.

ACKNOWLEDGMENTS

This work was funded by the European Office of Aerospace Research and Development (US Air Force Office of Scientific Research) within the project "From polymers to covalent glasses (PolGla)" (award no. FA8655-23-1-724). The PALS measurements were carried out within the framework of the "Unveiling the secrets of chemical TEMpering by POsitron annihilation Spectroscopy (TemPoS)" project. The specific heat experiments were funded by the National Science Centre Poland (grant no. UMO/2024/53/B/ST3/02514). Parts of this research were carried out at ELBE at the Helmholtz-Zentrum Dresden—Rossendorf e.V., a member of the Helmholtz Association. We would like to thank the facility staff and the positron team at ELBE (Ahmed G. Attallah) for assistance.

15512916, 2025, 12, Downloaded from https://ceramics.onlinelibrary.wiley.com/doi/10.1111/jace.20708 by Universita Di Trento, Wiley Online Library on [08/10/2025]. See the Terms and Conditions (https://onlinelibrary.wiley.com/terms-and-conditions) on Wiley Online Library for rules of use; OA articles are governed by the applicable Creative Commons License

Open access publishing facilitated by Universita degli Studi di Trento, as part of the Wiley - CRUI-CARE agreement.

ORCID

Mattia Biesuz https://orcid.org/0000-0002-4338-4177
Adane M. Abebe https://orcid.org/0000-0002-4430-0297
Sebastiano Mariazzi https://orcid.org/0000-0001-9985-8792
Roberto S. Brusa https://orcid.org/0000-0002-5239-7172
Daria Szewczyk https://orcid.org/0000-0001-7923-1239
Maik Butterling https://orcid.org/0000-0003-3674-0767
Maciej Oskar Liedke https://orcid.org/0000-0001-7933-7295
Andreas Wagner https://orcid.org/0000-0001-7575-3961
Eric Hirschmann https://orcid.org/0000-0001-5782-9627
Michele Cassetta https://orcid.org/0000-0003-2078-655X
Gian D. Sorarù https://orcid.org/0000-0002-0453-3379

REFERENCES

1. Colombo P, Mera G, Riedel R, Sorarù GD. Polymer-derived ceramics: 40 years of research and innovation in advanced ceramics. J Am Ceram Soc. 2010;93(7):1805–37. https://doi.org/10.1111/j.1551-2916.2010.03876.x
2. Sujith R, Jothi S, Zimmermann A, Aldinger F, Kumar R. Mechanical behaviour of polymer derived ceramics—a review. Int Mater Rev. 2021;66(6):426–49. https://doi.org/10.1080/09506608.2020.1784616
3. Vakifahmetoglu C, Zeydanli D, Colombo P. Porous polymer derived ceramics. Mater Sci Eng R: Rep. 2016;106:1–30. https://doi.org/10.1016/j.mser.2016.05.001
4. Rouxel T, Soraru G, Vicens J. Creep viscosity and stress relaxation of gel-derived silicon oxycarbide glasses. J Am Ceram Soc. 2001;84(5):1052–58.
5. Vallachira P, Zera E, Graczyk-Zajac M, Riedel R, Soraru GD. Structural design of polymer-derived SiOC ceramic aerogels for high-rate Li ion storage applications. J Am Ceram Soc. 2016;99(9):2977–83. https://doi.org/10.1111/jace.14323
6. Eckel ZC, Zhou C, Martin JH, Jacobsen AJ, Carter WB, Schaedler TA. Additive manufacturing of polymer-derived ceramics. Science (1979). 2016;351(6268):58–62. https://doi.org/10.1126/science.aad2688
7. Chaudhary RP, Parameswaran C, Idrees M, Rasaki AS, Liu C, Chen Z, et al. Additive manufacturing of polymer-derived ceramics: materials, technologies, properties and potential applications. Prog Mater Sci. 2022;128:100969. https://doi.org/10.1016/j.pmatsci.2022.100969
8. Greil P. Active-filler-controlled pyrolysis of preceramic polymers. J Am Ceram Soc. 1995;78(4):835–48. https://doi.org/10.1111/j.1151-2916.1995.tb08404.x
9. Karakuscu A, Guider R, Pavesi L, Sorarù GD. Broad-band tunable visible emission of sol–gel derived SiBOC ceramic thin films. Thin Solid Films. 2011;519(11):3822–26. https://doi.org/10.1016/j.tsf.2011.01.233
10. Guo A, Roso M, Modesti M, Liu J, Colombo P. Preceramic polymer-derived SiOC fibers by electrospinning. J Appl Polym Sci. 2014;131(3). https://doi.org/10.1002/app.39836
11. Jana P, Zera E, Sorarù GD. Processing of preceramic polymer to low density silicon carbide foam. Mater Des. 2017;116:278–86. https://doi.org/10.1016/j.matdes.2016.12.010
12. Manoj Kumar BV, Kim Y-W. Processing of polysiloxane-derived porous ceramics: a review. Sci Technol Adv Mater. 2010;11(4):044303. https://doi.org/10.1088/1468-6996/11/4/044303
13. Vakifahmetoglu C, Semerci T, Gurlo A, Soraru GD. Polymer derived ceramic aerogels. Curr Opin Solid State Mater Sci. 2021;25(4):100936. https://doi.org/10.1016/j.cossms.2021.100936
14. Stabler C, Ionescu E, Graczyk-Zajac M, Gonzalo-Juan I, Riedel R. Silicon oxycarbide glasses and glass-ceramics: "All-Rounder" materials for advanced structural and functional applications. J Am Ceram Soc. 2018;101:4817–56. https://doi.org/10.1111/jace.15932
15. Campostrini R, Zambotti A, Biesuz M, Sorarù GD. On the pyrolysis of a methyl-silsesquioxane in reactive CO_2 atmosphere: a TG/MS and FT-IR study. J Am Ceram Soc. 2021;105:2465–73. https://doi.org/10.1111/jace.18270
16. Widgeon SJ, Sen S, Mera G, Ionescu E, Riedel R, Navrotsky A. ^{29}Si and ^{13}C solid-state NMR spectroscopic study of nanometer-scale structure and mass fractal characteristics of amorphous polymer derived silicon oxycarbide ceramics. Chem Mater. 2010;22(23):6221–28. https://doi.org/10.1021/cm1021432
17. Bréquel H, Parmentier J, Walter S, Badheka R, Trimmel G, Masse S, et al. Systematic structural characterization of the high-temperature behavior of nearly stoichiometric silicon oxycarbide glasses. Chem Mater. 2004;16(13):2585–98. https://doi.org/10.1021/cm049847a
18. Wen Q, Yu Z, Riedel R. The fate and role of in situ formed carbon in polymer-derived ceramics. Prog Mater Sci. 2020;109:100623. https://doi.org/10.1016/j.pmatsci.2019.100623
19. Moldovan S, Ersen O, Sanchez C, Campostrini R, Sorarù GD. Shedding light onto the nano- and micro-structures of B-containing SiOC glasses using high resolution TEM 3D imaging. J Eur Ceram Soc. 2019;39(10):3042–50. https://doi.org/10.1016/j.jeurceramsoc.2019.03.044
20. Cassetta M, Peterlik H, Konegger T, Daldosso N, Sorarù GD, Biesuz M. Microporosity evolution in polymer-derived SiOC glasses pyrolyzed in different atmospheres. J Am Ceram Soc. 2024;107(8):5224–37. https://doi.org/10.1111/jace.19816
21. Sorarù GD, Girardini K, Narisawa M, Biesuz M. Effect of anionic substitution on the high temperature stability of polymer-derived SiOC glasses. J Am Ceram Soc. 2021;104:3097–104. https://doi.org/10.1111/jace.17691
22. Burns GT, Taylor RB, Xu Y, Zangvil A, Zank GA. High-temperature chemistry of the conversion of siloxanes to silicon carbide. Chem Mater. 1992;4(6):1313–23. https://doi.org/10.1021/cm00024a035
23. Narisawa M, Funabiki F, Iwase A, Wakai F, Hosono H. Effects of atmospheric composition on the molecular structure of synthesized silicon oxycarbides. J Am Ceram Soc. 2015;10:3373–80. https://doi.org/10.1111/jace.13756
24. Sorarù GD, Tavonatti C, Kundanati L, Pugno N, Biesuz M. Effect of the pyrolysis atmosphere on the mechanical prop-

15512916, 2025, 12, Downloaded from https://ceramics.onlinelibrary.wiley.com/doi/10.1111/jace.20708 by Universita Di Trento, Wiley Online Library on [08/10/2025]. See the Terms and Conditions (https://onlinelibrary.wiley.com/terms-and-conditions) on Wiley Online Library for rules of use; OA articles are governed by the applicable Creative Commons License

erties of polymer-derived SiOC and SiCN. J Am Ceram Soc. 2020;103(11):6519–30. https://doi.org/10.1111/jace.17392
25. Narisawa M, Funabiki F, Iwase A, Wakai F, Hosono H. Effects of atmospheric composition on the molecular structure of synthesized silicon oxycarbides. J Am Ceram Soc. 2015;10:3373–80. https://doi.org/10.1111/jace.13756
26. Sorarù GD, Tavonatti C, Kundanati L, Pugno N, Biesuz M. Effect of the pyrolysis atmosphere on the mechanical properties of polymer-derived SiOC and SiCN. J Am Ceram Soc. 2020;103(11):6519–30. https://doi.org/10.1111/jace.17392
27. Campostrini R, Zambotti A, Biesuz M, Sorarù GD. On the pyrolysis of a methyl-silsesquioxane in reactive CO_2 atmosphere: a TG/MS and FT-IR study. J Am Ceram Soc. 2022;105:2465–73. https://doi.org/10.1111/jace.18270
28. Lipowitz J. Structure and properties of ceramic fibers prepared from organosilicon polymers. J Inorg Organomet Polym. 1991;1(3):277–97. https://doi.org/10.1007/BF00702494
29. Lipowitz J, Rabe JA, Frevel LK, Miller RL. Characterization of nanoporosity in polymer-derived ceramic fibres by X-ray scattering techniques. J Mater Sci. 1990;25(4):2118–24. https://doi.org/10.1007/BF01045776
30. Konegger T, Drechsel C, Peterlik H. In-situ small angle X-ray scattering (SAXS)—a versatile tool for clarifying the evolution of microporosity in polymer-derived ceramics. Microporous Mesoporous Mater. 2021;324:111268. https://doi.org/10.1016/j.micromeso.2021.111268
31. Fontão NC, Ferrari LN, Sapatieri JC, Rezwan K, Wilhelm M. Influence of the pyrolysis temperature and TiO_2-incorporation on the properties of SiOC/SiC composites for efficient wastewater treatment applications. Membranes. 2022;12(2):175. https://doi.org/10.3390/membranes12020175
32. Wagner A, Butterling M, Liedke MO, Potzger K, Krause-Rehberg R. Positron annihilation lifetime and Doppler broadening spectroscopy at the ELBE facility. AIP Conf Proc. 2018;1970:040003. https://doi.org/10.1063/1.5040215
33. Hirschmann E, Butterling M, Hernandez Acosta U, Liedke MO, Attallah AG, Petring P, et al. A new system for real-time data acquisition and pulse parameterization for digital positron annihilation lifetime spectrometers with high repetition rates. J Instrumentation. 2021;16(08):P08001. https://doi.org/10.1088/1748-0221/16/08/P08001
34. Olsen JV, Kirkegaard P, Pedersen NJ, Eldrup M. PALSfit: a new program for the evaluation of positron lifetime spectra. Phys Status Solidi C. 2007;4(10):4004–6. https://doi.org/10.1002/pssc.200675868
35. Dull TL, Frieze WE, Gidley DW, Sun JN, Yee AF. Determination of pore size in mesoporous thin films from the annihilation lifetime of positronium. J Phys Chem B. 2001;105(20):4657–62. https://doi.org/10.1021/jp004182v
36. Lashley JC, Hundley MF, Migliori A, Sarrao JL, Pagliuso PG, Darling TW, et al. Critical examination of heat capacity measurements made on a quantum design physical property measurement system. Cryogenics (Guildf). 2003;43(6):369–78. https://doi.org/10.1016/S0011-2275(03)00092-4
37. Szewczyk D, Jeżowski A, Krivchikov AI, Tamarit JL. Influence of thermal treatment on thermal properties of adamantane derivatives. Low Temp Phys. 2015;41(6):469–72. https://doi.org/10.1063/1.4922101
38. Carini G, Carini G, Cosio D, D'Angelo G, Rossi F. Low temperature heat capacity of permanently densified SiO_2 glasses. Philos Mag. 2016;96(7–9):761–73. https://doi.org/10.1080/14786435.2015.1122845
39. Moysan C, Riedel R, Harshe R, Rouxel T, Augereau F. Mechanical characterization of a polysiloxane-derived SiOC glass. J Eur Ceram Soc. 2007;27:397–403. https://doi.org/10.1016/j.jeurceramsoc.2006.01.016
40. Mazo MA, Soriano D, Rubio J. Mechanical response of silicon oxycarbide materials processed by spark plasma sintering. Ceram Int. 2023;49(8):12866–75. https://doi.org/10.1016/j.ceramint.2022.12.158
41. Ni H, Li X, Gao H. Elastic modulus of amorphous SiO_2 nanowires. Appl Phys Lett. 2006;88(4):043108. https://doi.org/10.1063/1.2165275
42. Galusek D, Riley FL, Riedel R. Nanoindentation of a polymer-derived amorphous silicon carbonitride ceramic. J Am Ceram Soc. 2001;84(5):1164–66. https://doi.org/10.1111/j.1151-2916.2001.tb00806.x
43. Jambur V, Molina-Ruiz M, Dauer T, Horton-Bailey DJ, Vallery R, Gidley DW, et al. Temperature effects on the structure and mechanical properties of vapor deposited a-SiO_2. J Non Cryst Solids. 2022;587:121588. https://doi.org/10.1016/j.jnoncrysol.2022.121588
44. Ando MF, Fuhrmann S, Pan Z, Rodrigues BP, Mori T, Ebbinghaus SG, et al. Boson peak and structural heterogeneity in ternary SiO_2–Al_2O_3–B_2O_3 glasses. J Am Ceram Soc. 2021;104(10):4991–5000. https://doi.org/10.1111/jace.17771
45. Ando MF, Benzine O, Pan Z, Garden J-L, Wondraczek K, Grimm S, et al. Boson peak, heterogeneity and intermediate-range order in binary SiO_2–Al_2O_3 glasses. Sci Rep. 2018;8(1):5394. https://doi.org/10.1038/s41598-018-23574-1
46. Stabler C, Reitz A, Stein P, Albert B, Riedel R, Ionescu E. Thermal properties of SiOC glasses and glass ceramics at elevated temperatures. Materials. 2018;11(2):279. https://doi.org/10.3390/ma11020279
47. Asheghi M, Touzelbaev MN, Goodson KE, Leung YK, Wong SS. Temperature-dependent thermal conductivity of single-crystal silicon layers in SOI substrates. J Heat Transfer. 1998;120(1):30–36. https://doi.org/10.1115/1.2830059
48. Stabler C, Reitz A, Stein P, Albert B, Riedel R, Ionescu E. Thermal properties of SiOC glasses and glass ceramics at elevated temperatures. Materials. 2018;11(2):279. https://doi.org/10.3390/ma11020279
49. Sorarù GD, Girardini K, Narisawa M, Biesuz M. Effect of anionic substitution on the high temperature stability of polymer-derived SiOC glasses. J Am Ceram Soc. 2021;104:3097–104. https://doi.org/10.1111/jace.17691
50. Rouxel T, Soraru G, Vicens J. Creep viscosity and stress relaxation of gel-derived silicon oxycarbide glasses. J Am Ceram Soc. 2001;84(5):1052–58.
51. Turquat C, Kleebe H, Gregori G, Walter S, Sorarù GD. Transmission electron microscopy and electron energy-loss spectroscopy study of nonstoichiometric silicon–carbon–oxygen glasses. J Am Ceram Soc. 2001;84(10):2189–96. https://doi.org/10.1111/j.1151-2916.2001.tb00986.x
52. Santhosh B, Biesuz M, Sorarù GD. Thermal properties of dense polymer-derived SiCN(O) glasses. Mater Lett. 2021;288:129336. https://doi.org/10.1016/j.matlet.2021.129336

15512916, 2025, 12, Downloaded from https://ceramics.onlinelibrary.wiley.com/doi/10.1111/jace.20708 by Universita Di Trento, Wiley Online Library on [08/10/2025]. See the Terms and Conditions (https://onlinelibrary.wiley.com/terms-and-conditions) on Wiley Online Library for rules of use; OA articles are governed by the applicable Creative Commons License

53. Li Z, Wang Y, An L. Control of the thermal conductivity of SiC by modifying the polymer precursor. J Eur Ceram Soc. 2017;37(1):61–67. https://doi.org/10.1016/j.jeurceramsoc.2016.08.023
54. Gurlo A, Ionescu E, Riedel R, Clarke DR. The thermal conductivity of polymer-derived amorphous Si–O–C compounds and nano-composites. J Am Ceram Soc. 2016;99(1):281–85. https://doi.org/10.1111/jace.13947
55. Gengler JJ, Hu J, Jones JG, Voevodin AA, Steidl P, Vlček J. Thermal conductivity of high-temperature Si–B–C–N thin films. Surf Coat Technol. 2011;206(7):2030–33. https://doi.org/10.1016/j.surfcoat.2011.07.058
56. Göbel A, Hemberger F, Ebert H-P, Jansen M, Wilfert J. Thermophysical properties of an amorphous polymer-derived Si/B/N/C ceramic. Thermochim Acta. 2011;520(1–2):20–24. https://doi.org/10.1016/j.tca.2011.03.001

SUPPORTING INFORMATION

Additional supporting information can be found online in the Supporting Information section at the end of this article.

How to cite this article: Biesuz M, Abebe AM, Karacasulu L, Mariazzi S, Brusa RS, Szewczyk D, et al. From polymer to SiOC glass: structure, microstructure, mechanical, and thermal properties. J Am Ceram Soc. 2025;108:e20708. https://doi.org/10.1111/jace.20708

15512916, 2025, 12, Downloaded from https://ceramics.onlinelibrary.wiley.com/doi/10.1111/jace.20708 by Universita Di Trento, Wiley Online Library on [08/10/2025]. See the Terms and Conditions (https://onlinelibrary.wiley.com/terms-and-conditions) on Wiley Online Library for rules of use; OA articles are governed by the applicable Creative Commons License